Geol. Mag. **154** (*5*), *2017, pp. 1171–1186.* © *Cambridge University Press 2017*
doi:10.1017/S0016756817000267

Influence of Hegenshan–Heihe suture on evolution of late Mesozoic extensional structures in Wunite depression, Erlian Basin, Inner Mongolia, China

QUANYUN MIAO*†, JIAFU QI*†, LISHUANG WANG*, SHUAI ZHANG* & XIULI WEI‡

*State Key Laboratory of Petroleum Resource and Prospecting, China University of Petroleum, Beijing 102249, PR China
‡Exploration Department of PetroChina Huabei Oilfield Company, Renqiu, Hebei 062550, PR China

(*Received* 10 August 2016; *accepted* 28 February 2017; *first published online* 5 April 2017)

Abstract – We integrate previous work on the Hegenshan–Heihe suture with our interpretation of geomagnetic anomaly and seismic reflection data to investigate the role of the Hegenshan–Heihe suture in the evolution of late Mesozoic extensional structures in the Wunite depression of the Erlian Basin. Sags in the Wunite depression present as NE50° trending in the western sector, N0°–NE30° trending in the central sector and NE45° trending in the eastern sector. Our results highlight the importance of the pre-existing Hegenshan–Heihe suture in the evolution of the late Mesozoic rift system and reveal the following details. (1) The NE50° extent sags in the western sector are controlled by the *c.* NE50°-trending suture. Moreover, the extensional deformation of the reactivated suture during Early Cretaceous time resulted in a further vertical and horizontal extension of major border faults. (2) The N0°–NE30° extent sags in the central sector are influenced by the *c.* NE75°-trending suture. The sinistral strike-slip component of the reactivated suture during Early Cretaceous time resulted in a strike rotation of major border faults from NEE-trending (following the suture) to NNE-trending. (3) Because of strike-slip deformation, which resulted from the deformation of the reactivated suture accrued in major border faults, light dip-slip deformation led to less vertical offset. (4) The NE45°-trending sags in the eastern sector are controlled by the *c.* NE45°-trending suture. Moreover, the extensional deformation of the reactivated suture during Early Cretaceous time facilitated a further vertical and horizontal prolongation of major border faults.

Keywords: Erlian Basin, Wunite depression, pre-existing structure, Hegenshan–Heihe suture, late Mesozoic

1. Introduction

Pre-existing structures play an important role in the evolution of a rift basin, and their effects on extensional structures in a basin have been investigated by many geologists (McConnell, 1972; Dunbar & Sawyer, 1988; Milani & Davison, 1988; Quinlan *et al.* 1993; Jutz & Chorowicz, 2010; Lasky & Glikson, 2011). Numerous laboratory experiments have been conducted to study the role of pre-existing structure geometry on fault activation in rift basins (McClay & White, 1995; Bonini *et al.* 1997; Higgins & Harris, 1997; Keep & McClay, 1997; Schlische, Withjack & Eisenstakt, 2002; Corti *et al.* 2011). Recently, 'Mohr space' has been proposed to investigate the influence of pre-existing structures on the formation and evolution of rift basins (Tong & Yin, 2011; Tong *et al.* 2014). Although some laboratory experiments have modelled fault systems using natural datasets, such as in the Gulf of California, the Revfallet fault system offshore of Norway and the Eastern Alps (Withjack & Jamison, 1986; Dooley, McClay & Pascoe, 2003; Rosenberg *et al.* 2007), the variety of pre-existing weaknesses in the models is limited. The analysis of natural systems is therefore particularly significant for rift basin research.

It is widely accepted that the Central Asian Orogenic Belt (CAOB) is one of the largest accretionary orogens in the world. It separates the Siberian craton from the Tarim and Sino-Korean cratons (Sengör, Natal'in & Burtman, 1993; Windley *et al.* 2007; Su *et al.* 2012; Wilhem, Windley & Stampfli, 2012; Li *et al.* 2014; Xu *et al.* 2015; Shi *et al.* 2016) (Fig. 1a). The Xing'an–Mongolia Orogenic Belt (XMOB) is the eastern segment of the CAOB. It extends across the Inner Mongolia, Heilongjiang, Jilin and Liaoning provinces of NE China (Jian *et al.* 2012; Zeng *et al.* 2012; Xu *et al.* 2015) (Fig. 1b).

Recently, Liu *et al.* (2017) gave a tectonic division of XMOB by researching previous works. They suggest the Palaeozoic tectonic divisions are Erguna (Argun in some references) block, Xing'an block, Songliao block, Jiamusi block and Xinlin–Xiguitu suture, Hegenshan–Heihe suture (Zhou *et al.* 2011, 2014, 2015; Sun *et al.* 2013; J. Han et al. 2015;) (Erenhot–Hegenshan in some references), Mudanjiang suture

†Authors for correspondence: mqycup@163.com; qijiafu@cup.edu.cn

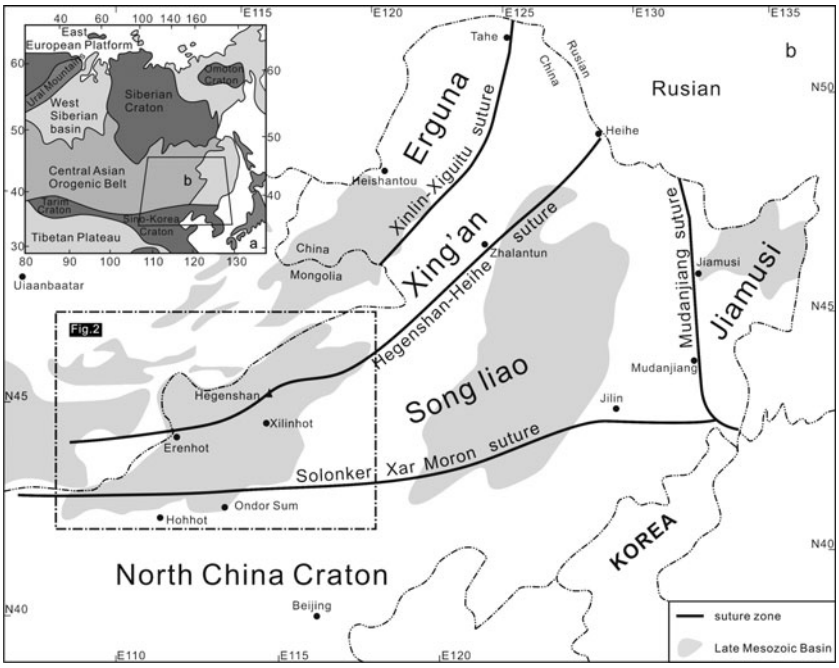

Figure 1. Palaeozoic blocks, sutures and late Mesozoic rift basins in XMOB, NE China: (a) location of the CAOB (modified after Xu *et al.* 2015); (b) blocks and sutures in the XMOB and adjacent area emphasizing the location of Erlian Basin and Hegenshan–Heihe suture (modified after Robinson *et al.* 1999; Miao *et al.* 2008; Han *et al.* 2017; Li *et al.* 2017).

and Solonker Xar Moron suture (Robinson *et al.* 1999; Xiao *et al.* 2003; Miao *et al.* 2008; Wang *et al.* 2015) (Ondor Sum–Yanji in some references).

Sutures, which record the closure of the Palaeo-Asian Ocean (Han *et al.* 2012), are vital to the study of evolution of Palaeo-Asian Ocean. In recent years, some works have proved the location and extension of some sutures. Firstly, Xinlin–Xiguitu suture is indeed the dividing line of the Erguna and Xing'an blocks, proven by the Lower Palaeozoic post-orogenic A-type granites which discontinuously crop out along it (Ge *et al.* 2005), Hf isotopic analysis (Zhang *et al.* 2013), Tayuan gabbros (Feng *et al.* 2014), Jifeng ophiolitic (647 Ma) (Feng *et al.* 2016) and the detrital zircon studies of Devonian and Carboniferous sediments in Yimin area (G. Han *et al.* 2015). Secondly, the Hegenshan–Heihe suture represents the dividing line between the Xing'an and Songliao blocks (Miao *et al.* 2008). The eastern extension of the Hegenshan–Heihe suture was under hot debate (Zhang *et al.* 1994; Li, 1998; Li *et al.* 2009) until Han *et al.* (2012) sought the eastern extension by tracing the provenance information of the magmatic arc from Permian sandstones. Han *et al.* (2012) proved that the eastern extension of the Hegenshan–Heihe suture started from Erenhot in west, via Hegenshan Inner Mongolia, to Zhalantun and then to Heihe in Heilongjiang province. Liu *et al.* (2017) obtained a similar opinion as Han *et al.* (2012) by studying the palaeogeography on either side of the Hegenshan–Heihe suture. Thirdly, Mudanjiang suture is the dividing line between the Songliao and Jiamusi blocks (Fig. 1b). It is a high-*P*/*T* metamorphosed tectonic mélange produced from the subduction/collision between these two blocks, aligned approximately N–S. It was cut by two faults, namely the Yilan–Yitong and Dunhua–Mishan faults, during Mesozoic time (Zhou *et al.* 2014; Liu *et al.* 2017). Fourthly, Solonker Xar Moron suture, the most important suture of XMOB, has been proven to be the final closure site of the Palaeo-Asian Ocean from new data in the last decades (Xiao *et al.* 2003; Li, 2006; Zhang *et al.* 2006; Wu *et al.* 2007; Xiao, Kröner & Windley, 2009; Jian *et al.* 2010; G. Han *et al.* 2015; Xiao, Sun & Santosh, 2015). The suture records the closure of the Palaeo-Asian Ocean according to the Palaeozoic strata on either side of the Xar Moron River (Wang & Fan, 1997; Sun *et al.* 2004). The eastern part is cut by the Yilan–Yitong and Dunhua–Mishan faults (Zhou *et al.* 2014; Liu *et al.* 2017).

During late Mesozoic time, large-scale rift basins developed on these blocks and sutures. The Erlian Basin is one of these rift basins (Fig. 1b). It superimposes the western parts of the Xing'an and Songliao blocks and the western segments of the Hegenshan–Heihe and Solonker Xar Moron sutures (Fig. 1b). The segment of the Hegenshan–Heihe suture in the Erlian Basin extends from Erenhot in the SW via Hegenshan to Holinhot in the NE (Figs 1b, 2, 3; see Section 2.b). Previous studies of the Hegenshan–Heihe suture in this area concentrated on the geochemistry and geochronology (Robinson *et al.* 1999; Xiao *et al.* 2003; Miao *et al.* 2008). Although some published data on ophiolites along the suture (Robinson *et al.* 1999; Miao *et al.* 2008) have revealed potential orientation changes in the Hegenshan–Heihe suture, especially in the Wunite depression of the Erlian Basin (Fig. 4), little attention has been paid to the geometry analyses of the Hegenshan–Heihe suture and

https://doi.org/10.1017/S0016756817000267 Published online by Cambridge University Press

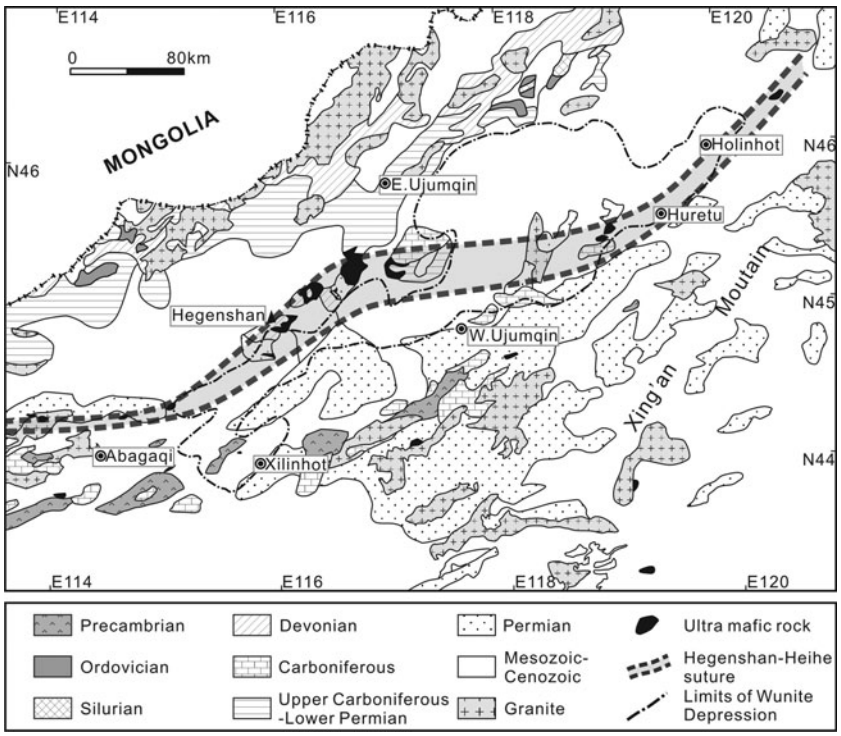

Figure 2. Geological map of the study region. Note the distribution of ophiolites (modified from Robinson *et al.* 1995, 1999; Miao *et al.* 2008) and the horizontal stretch of Hegenshan–Heihe suture. Outcrops of stratum are modified from Zhang *et al.* (2014).

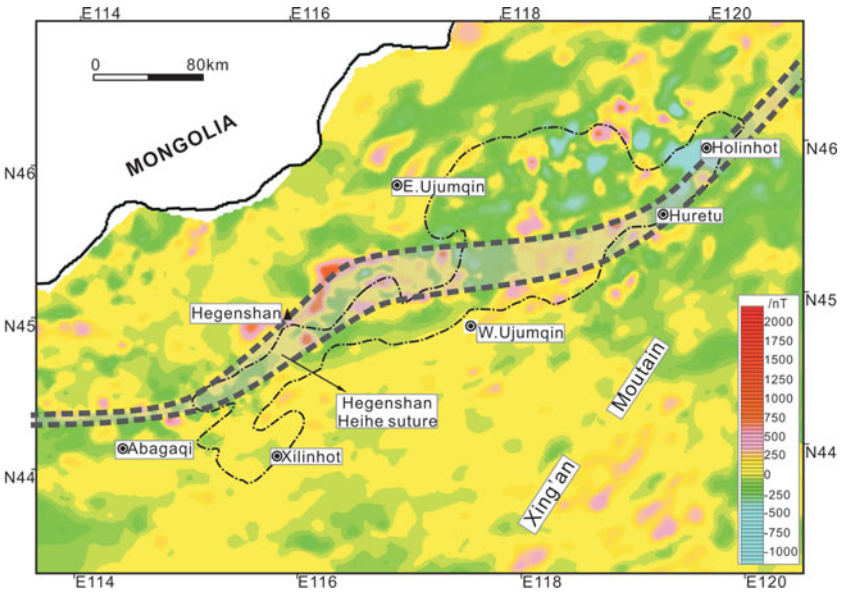

Figure 3. (Colour online) Geomagnetic anomaly of Wunite depression and surrounding areas to highlight the trend of the Hegenshan–Heihe suture. The Hegenshan–Heihe suture presents an obviously positive anomaly belt with different anomaly field on each sides.

the role of the suture on the overlying extensional structures.

In this paper, in order to investigate the role of the Hegenshan–Heihe suture on the late Mesozoic extensional structures, we analysed the horizontal trend and the kinematics of the Hegenshan–Heihe suture in the Wunite depression area of the Erlian Basin according to published data on ophiolites, strata on either side of the suture (Fig. 2) and geomagnetic anomalies (Fig. 3). We also analysed the architecture and major fault geometry of late Mesozoic sags according to seismic reflection data. We discuss the influence of the Hegenshan–Heihe suture on the late Mesozoic extensional structure.

2. Geological setting

2.a. Early Cretaceous feature of Erlian Basin

The late Mesozoic period was one of widespread intracontinental NW–SE-directed extension in NE China (Ma *et al.* 1983; Ren, Li & Jiao, 1998; Shao, Mu &

https://doi.org/10.1017/S0016756817000267 Published online by Cambridge University Press

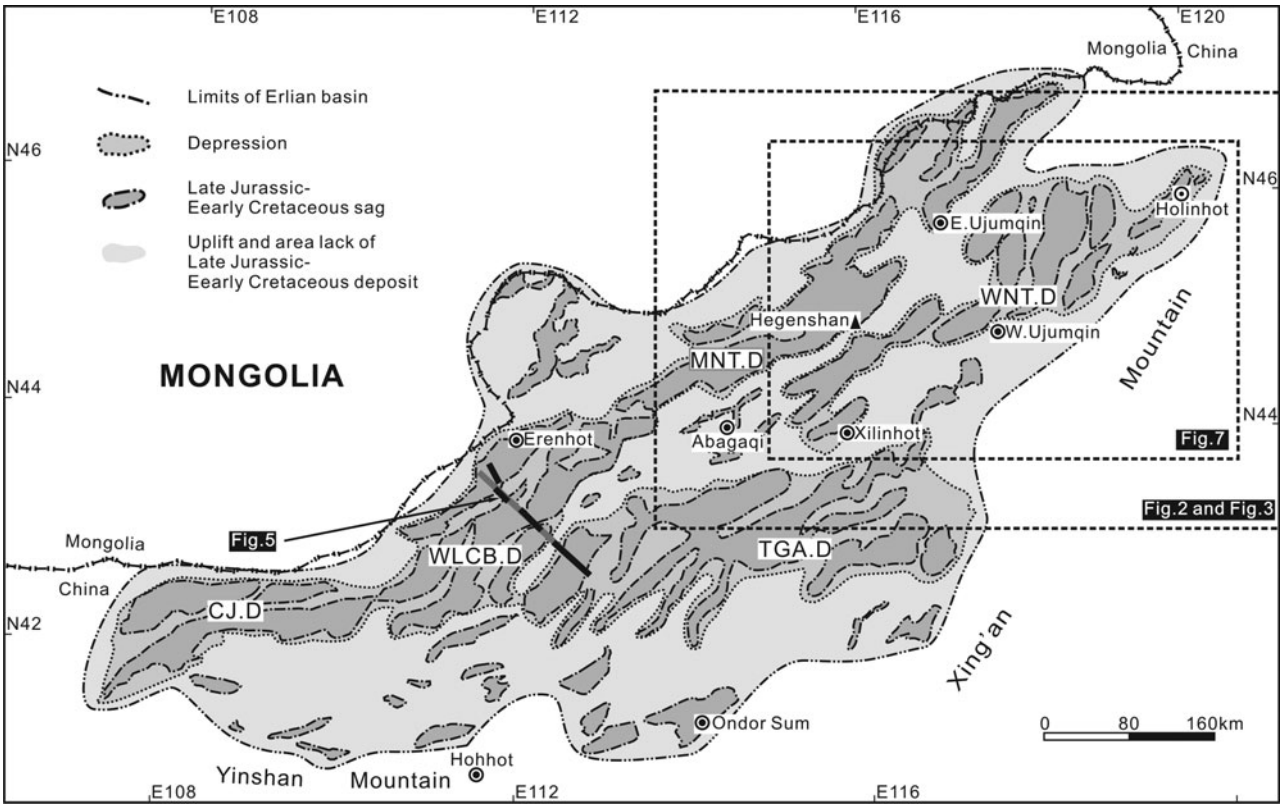

Figure 4. Diagram showing subsurface distribution of Late Jurassic – Early Cretaceous sags of the Erlian Basin (based on the seismic data from PetroChina Huabei Oilfield Company). Study area, Wunite Depression, is located in the NE of the basin. WNT.D – Wunite Depression; MNT.D – Manite depression; TGA.D – Tenggar depression; WLCB.D – Wulanchabu depression; CJ.D – Chuanjing depression (modified from Qi *et al.* 2015).

Zhang, 2000; Xiao, Yang & Chen, 2001; Wang *et al.* 2007; Meng *et al.* 2013). The extensional tectonics in the XMOB are verified by the large-scale concurrence of extensional basins (Song & Dou, 1997; Graham *et al.* 2001), metamorphic core complexes (Zheng, Wang & Wang, 1991; Webb *et al.* 1999) and rift-related magmatism (Wu, Sun & Lin, 1999; Zhu *et al.* 1999; Shao, Mu & Zhang, 2000). For the origin of the late Mesozoic widespread extensional movements in the XMOB , two points are prevalent. These can be interpreted as being produced by (a) back-arc extension caused by the subduction of the Pacific Plate under the Eurasian Plate (Watson *et al.* 1987; Traynor & Sladen, 1995; Ren, Li & Jiao, 1998; Ratschbacher *et al.* 2000; Xiao, Yang & Chen 2001) and (b) the break-off of the northwards-subducting Mongol–Okhotsk oceanic slab (Meng *et al.* 2002, 2003; Meng, 2003).

The Erlian Basin is certainly the product of extensional movement during late Mesozoic time; the major rifting period was during Late Jurassic – Early Cretaceous time (Graham *et al.* 2001; Xiao, Yang & Chen 2001; Meng *et al.* 2003). The basin basement has undergone multi-tectonic processes including Caledon, Hercynian, Indosinian and early Yanshan movements. Due to tectonic inversion at the end of Late Cretaceous time, most Upper Cretaceous sediments were denuded and relatively thin sediments conserved in partial sags (Dou & Chang, 2003; Meng *et al.* 2002).

The eastern boundary of the Erlian Basin is Xing'an Mountain, the southern boundary is the Yinshan and Yanshan mountains and the northwestern boundary is proximate to the border of China and Mongolia (Fig. 4). It has a total area of *c.* 100 000 km^2 (Dou & Chang, 2003). The Erlian Basin contains more than 50 sags that are controlled by high-angle normal faults or strike-normal faults (Figs 5, 6), with multi-clustered sags as the negative subordinate unit as depressions and a few scattered over the uplift (Fei, 1985; Wang, 1986; Yu, 1990; Li, Lu & Lin, 1997; Qi *et al.* 2015) (Fig. 4). The study area of this paper is the Wunite depression in the NE of the Erlian Basin (Fig. 4).

The rift stratigraphic sequences of the Erlian Basin comprise Upper Jurassic – Lower Cretaceous strata. They are separated by two regional unconformities from the underlying and overlying successions (Graham *et al.* 2001; Meng *et al.* 2003). The Upper Jurassic stratigraphy is the pre-rift sequence (Figs 5, 6), predominantly containing voluminous volcanic rocks of the Xinganling Group with sedimentary interbeds (Meng *et al.* 2003). The equivalents of the Xinganling Group in Western Liaoning have been well dated by $^{40}Ar/^{39}Ar$ and K/Ar methods to give an age of *c.* 145–156 Ma (Chen & Chen, 1997; Wang *et al.* 2006). The Lower Cretaceous contains multi-cycled sedimentary sequences. These are of the Aershan Formation (K_1ba) at the bottom, the Tenggar Formation (K_1bt) at the middle and the Saihantala Formation (K_1bs) at the

https://doi.org/10.1017/S0016756817000267 Published online by Cambridge University Press

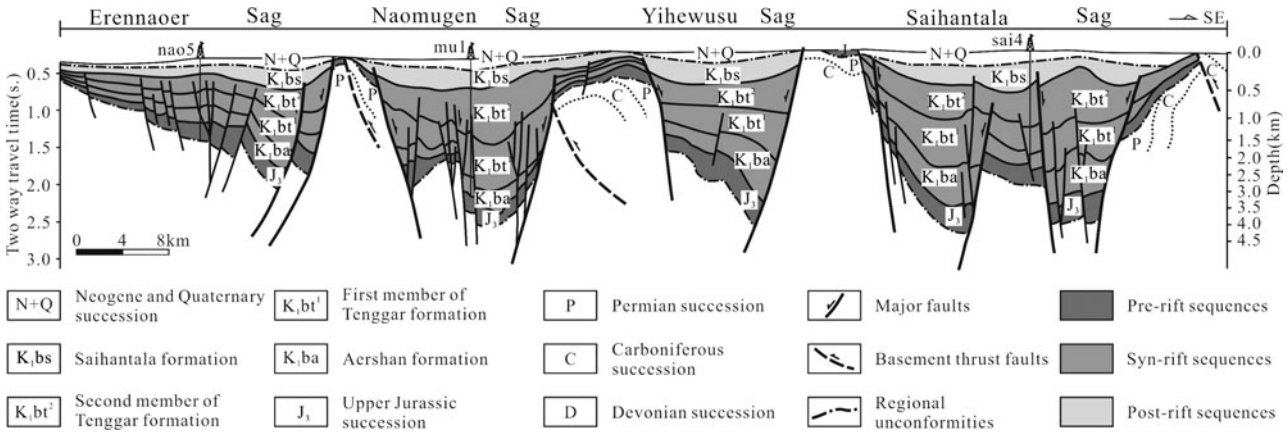

Figure 5. Cross-section of Erlian Basin shows the basic graben and half-graben geometry of sags and the three main rift sequences.

top (Graham *et al.* 2001; Meng *et al.* 2003) (Figs 5, 6). The Aershan and Tenggar formations comprise the syn-rift sequences (Dou, 1997; Lin *et al.* 2001; Meng *et al.* 2003). During the syn-rift period, major border faults showed dramatic activity and typically became linked, through-going and often corrugated faults (Meng *et al.* 2003). The Tenggar Formation is divided into two members: the first member (K_1bt^1) (Figs 5, 6) mainly contains sand/mudstone; and the second member (K_1bt^2) (Figs 5, 6) mainly comprises conglomerate and coal measure strata (Fei, 1985). The Saihantala Formation is the post-rift sequence and shows integral down-warping geometry (Figs 5, 6).

2.b. Hegenshan–Heihe suture in Wunite depression

After the overprinting of the strong Mesozoic deformation along Xing'an and Songliao blocks, it is not easy to trace the amalgamation between them. Fortunately, some geologists have used the distribution of the magnetic and gravitational anomaly (geophysical abnormal belt) and magmatic arc to trace the suture. Based on the genetic relation between the magmatic arc and the 'Hegenshan Ocean', Han *et al.* (2012) inferred that the Hegenshan–Heihe suture extended from Erenhot, via Hegenshan ophiolite, via Zhalantun and then to Heihe in the north of a magmatic arc traced by the provenance information of the magmatic arc from Permian sandstones. Zhou *et al.* (2015) revealed that the suture extended from Erenhot via Hegenshan when researching the emplacement time of the Hegenshan ophiolite. Recently, Liu *et al.* (2017) proved that the Hegenshan–Heihe suture extended along Erenhot via Hegenshan to Heihe by palaeogeographical studies. In their study, the distributions of lithofacies were obviously different on the either side of the Hegenshan–Heihe suture during Late Carboniferous and early and middle Permian time. A volcanic arc/belt developed along the Hegenshan–Heihe suture during Late Carboniferous – early Permian time (Liu *et al.* 2017). Work in the last decades has revealed that the Hegenshan–Heihe extended from Erenhot via Hegenshan to Heihe, and is the single suture of the Xing'an and the Songliao blocks (Miao *et al.* 2008; Han *et al.* 2012; Zhou *et al.* 2015; Liu *et al.* 2017).

The Wunite depression is located in the NE area of the Erlian Basin (Fig. 4). The majority of our study region is covered by Cenozoic sediments, and a few basement rocks, including Permian and Carboniferous sediments, are exposed. Around the Wunite depression, basement rocks are largely exposed and are intruded by igneous rocks (Fig. 2) resulting from multiple magmatic events (Zhang *et al.* 2014). A series of ophiolites is exposed in Abagaqi, Hegenshan and the eastern Xilinhot and Huretu areas (Fig. 2). Ophiolites, remnants of vanished oceans, generally mark the oceanic suture zone (Dewey, 1977; Şengör, 1992; Tortorici, Catalano & Carmelo, 2008; Xiao *et al.* 2014). However, it is not easy to analyse the trend of the Hegenshan–Heihe suture simply from the outcrops of ophiolite. In this paper, we combine the outcrops of strata with geomagnetic anomalies to study the azimuth of the Hegenshan–Heihe suture in the Wunite depression.

A geological map reveals that Precambrian metamorphic rocks are exposed in the south of the Wunite depression, whereas much younger strata are exposed NW of the Wunite depression (Fig. 2). Exposed Precambrian rocks belong to the Precambrian metamorphic basement which has an affinity to the Songliao block (Zhang *et al.* 2006). The data for the Xing'an block basement indicate a younger age (Miao *et al.* 2004, 2007; Sun *et al.* 2014), meaning that the Hegenshan–Heihe suture passes through the Wunite depression. A geomagnetic anomaly shows a significant positive belt distribution to the north of Abagaqi, Xilinhot, west Ujumqin and Huretu, via the Hegenshan area. The positive geomagnetic anomaly in the Hegenshan area is mainly caused by ophiolite. The extent of the magnetic anomaly reveals that the ophiolites undersurface are greater in volume than the exposed bodies. The other positive anomaly might be caused by some unexposed geological anomalous bodies or granite. Magnetic anomaly fields show different features on

https://doi.org/10.1017/S0016756817000267 Published online by Cambridge University Press

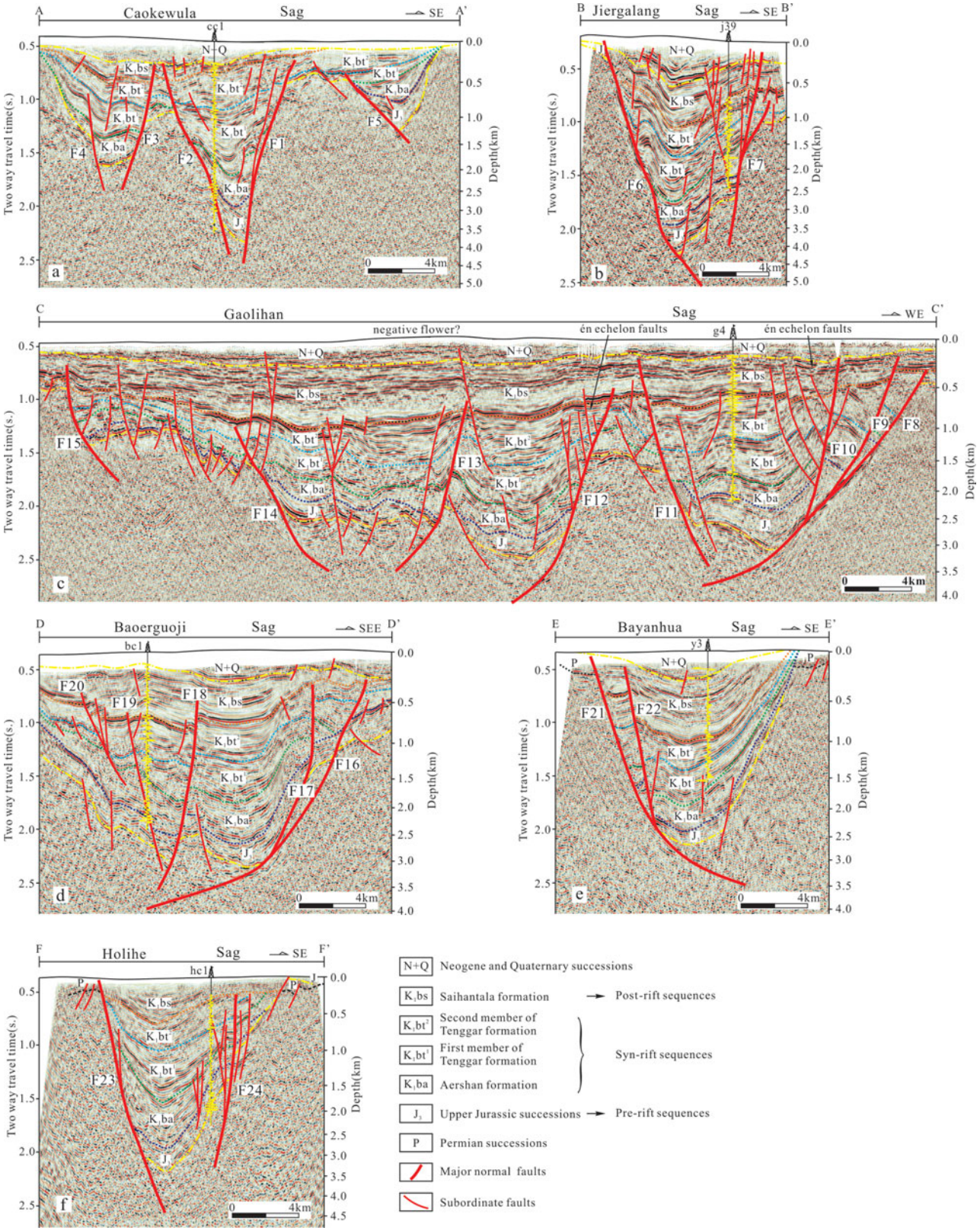

Figure 6. (Colour online) Interpreted seismic sections in western, central and eastern sectors crossing (a) the south sub-sags of Chaokewula sag; (b) the south sub-sag of Jiergalang sag; (c) the north sub-sags of Gaolihan sag; (d) the central sub-sag of Baoerguoji sag; (e) the south sub-sag of Bayanhua sag; and (f) the south sub-sag of Holihe sag. The depth is calculated by the velocity of the well in each section.

https://doi.org/10.1017/S0016756817000267 Published online by Cambridge University Press

the either side of the positive anomaly belt. The north anomaly field has a relatively uniformly distributed positive and negative anomaly, with amplitude from *c.* –400 to 500 nT. The south anomaly field mainly shows a positive and slightly negative anomaly near Xing'an Mountain and the south of Abagaqi, of amplitude *c.* –200 to 350 nT.

By combining previous research (Miao *et al.* 2008; Han *et al.* 2012; Zhou *et al.* 2015; Liu *et al.* 2017) with analysis of the magnetic anomaly (Fig. 2), the strata on either side of the suture and the ophiolites along the suture (Fig. 3), the horizontal trend of the Hegenshan–Heihe suture in Wunite depression can be divided into three segments (Figs 2, 3). The western segment trends from Abagaqi to the north of Hegenshan area with orientation *c.* NE50° and length *c.* 200 km; the middle segment trends from the north of the Hegenshan area to Huretu with orientation *c.* NE75° and length *c.* 190 km; and the eastern segment trends from Huretu to Holinhot with orientation *c.* NE45° and length *c.* 120 km (Fig. 2).

The largest exposed ophiolite is located in the Hegenshan area. Much work relating to the geochemistry on these massifs has been carried out (Robinson *et al.* 1995, 1999; Badarch, Gunningham & Windley, 2002; Nozaka & Liu, 2002; Miao *et al.* 2008). Recently, the Early Carboniferous (*c.* 354–333 Ma) and the Early Cretaceous (*c.* 142–125 Ma) mantle-melting episodes were documented via the SHRIMP zircon and geochemical study of the Hegenshan ophiolites (Jian *et al.* 2012). In other words, being the pre-existing structure of the Wunite depression, the Hegenshan–Heihe suture reactivated during Early Cretaceous time. Under regional extension in the NW–SE direction, the Hegenshan–Heihe suture underwent differing deformation in different areas due to the varying orientation. The western and eastern segments mainly underwent extensional deformation, whereas the middle segment underwent transtensional extension.

3. Materials and methods

We use seismic reflection data to describe the distribution and geometric features of the late Mesozoic faults that controlled the development of sags in the Wunite depression. Most major faults (Fig. 7) are constrained by two-dimensional (2D) seismic reflection data collected by PetroChina Huabei Oilfield for petroleum exploration. Generally, the line spacing of the 2D seismic data is between 1 and 2 km. A few areas (central in the Jiergalang sag) are interpreted by 3D seismic reflection data. Six representative seismic profiles are chosen and six wells are used to constrain the stratigraphy and seismic velocities within the upper part of the profiles. Typically, 2.5 s two-way time (TWT) of the seismic record is presented with 0.5 s TWT in elevation. The depth of the sag is converted using the velocities of the chosen wells.

4. Late Mesozoic extensional structures

The Wunite depression extends *c.* NE50°. Based on seismic reflection data, it is divided into 10 sags (Fig. 7). Each sag has an independent sedimentary system with multiple provenances (Zhang, 1998; Kuang *et al.* 2013). They occur at various scales with lengths ranging from *c.* 40 to *c.* 150 km and widths from several kilometres to *c.* 50 km. A relatively large sag usually consists of several smaller sags. Compounded types can be categorized as serial, parallel and en échelon based on the major border faults patterns. The serial and parallel types have more than two major border faults of the same orientation and are linked to each other or extend in parallel. The en échelon type has more than two major border faults extending en échelon in right or left steps (Meng *et al.* 2012). Cross-sections of the sags usually present half-graben geometry, and major border faults show listric geometry (Fig. 6). The depocentres of sags commonly extend along major border faults (Fig. 7). Variations in the fault patterns and the architecture of sags in the Wunite depression can be observed, allowing the identification of three sectors: the western, central and eastern sectors (Fig. 7).

The western sector is composed of four sags: Chaokewula, Jiergalang, Baiyinhushuo and Buridun (1, 2, 3 and 4, respectively, in Fig. 7) with a predominant NE50° trending. The length of each sag is more than 50 km and the width is less than 20 km. Sags commonly extend in series or parallel. Subordinate antithetic faults (dipping contrary to the major border fault) usually develop in the western sector (Fig. 7). These faults commonly promote further subsidence of sediments in the sags (Luo *et al.* 2005). For example, Chaokewula (Figs 6a, 7) is compounded by more than five sub-sags in series or parallel, with lengths of *c.* 106 km and widths of *c.* 20 km. A seismic section across the southern region reveals that three sub-sags are controlled by five high-angle normal faults (Fig. 6a). Fault F1 is the major border fault that controls the development and evolution of the sag. Fault F2 is the subordinate antithetic fault that delimits the central sub-sag associated with fault F1. Faults F3, F4 and F5 control the other two sub-sags (Fig. 6a). The activity of F2 results in the further subsidence of sediments in the central sub-sag. The lowest depth of the Jurassic stratigraphy in the central sub-sag is *c.* 4000 m, and the thickness of pre-rift and syn-rift sediments (the total thickness from the Jurassic stratigraphy to Tenggar formations) is *c.* 3500 m. A further example is Jiergalang (Figs 6b, 7), which is composed of two sub-sags. The length is *c.* 60 km and the width *c.* 16 km. A seismic section across the north sub-sag reveals that Jiergalang is totally controlled by Fault F6 and subordinate antithetic fault F7 (Fig. 6b). Faults F6 and F7 are both high-angle normal faults and control the sedimentary filling in the north sub-sag. The lowest depth of the Jurassic stratigraphy is *c.* 4100 m, and the thickness of pre-rift and syn-rift sediments is

https://doi.org/10.1017/S0016756817000267 Published online by Cambridge University Press

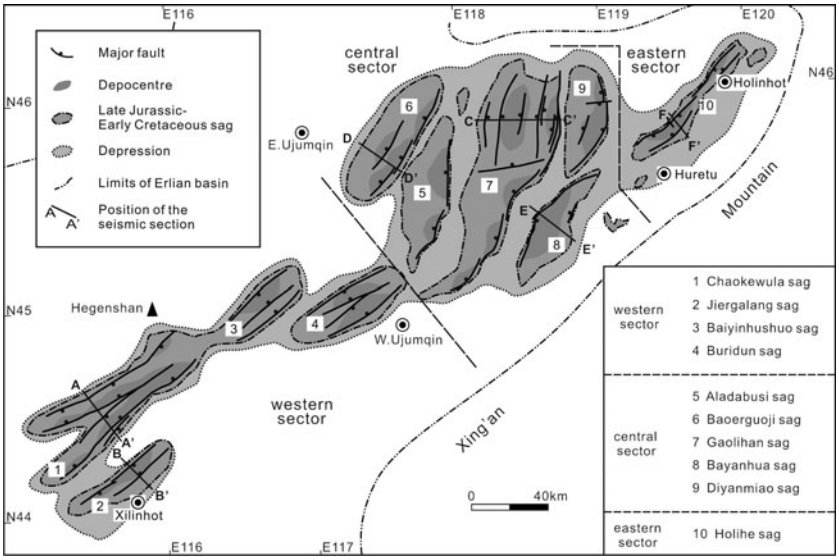

Figure 7. Framework of Wunite depression showing the distribution of western, central and eastern sectors and the major faults, depocentres of sags. Major faults include major border faults and major subordinate faults that control the sediments filling. Sags in the western sector are *c.* NE50° trending, in the central sector predominantly NE0°–NE30° trending and in the eastern sector *c.* NE45°-trending.

c. 3200 m. Sags in the western sector are typically narrow with deep and long geometry.

The central sector includes five sags: Aladabusi, Boerguoji, Gaolihan, Diyanmiao and Bayanhua (5, 6, 7, 8 and 9, respectively, in Fig. 7), predominantly NE0°–NE30° trending. The minimum width of sags in this sector is more than 20 km. For example, Gaolihan is the largest sag and has a maximum width of *c.* 50 km (Figs 6c, 7). It has developed five sub-sags: four are half-grabens aligning in a right step en échelon and the other is an asymmetrical graben that extends parallel to the north half-graben (Fig. 7). A seismic profile crossing the north part of Gaolihan (Fig. 6c) shows that the two parallel sub-sags are generally N–S trending and are separated by a lower salient. Fault F8 is the major border fault controlling the evolution of the sag. Faults F9 and F10, synthetic branches of fault F8, bottom out to F8 at a depth of *c.* 2700 m. Fault F11 is an antithetic fault and shows little control over the deposition of sediments. Faults F12, F13 and F14 control the development of the asymmetric graben, whereas fault F15 controls the western fault-step zone (Fig. 6c). Most of these major faults gradually slow down and slip at *c.* 3500 m, or a shallower level. Although a series of antithetic faults such as F11, F14 and F15 develops in these sub-sags, they rarely control the sedimentary filling (Fig. 6c). Synthetic faults constrain further subsidence, but extend the horizontal range of sags. In Gaolihan sag, the lowermost depth of the Jurassic stratigraphy is *c.* 3200 m. The maximum thickness of pre-rift and syn-rift sediments is *c.* 2300 m (Fig. 6c). Baoerguoji is the second-largest sag in the central sector. It consists of three sub-sags in right step en échelon (Fig. 7). A seismic profile reveals that the central sub-sag also shows half-graben geometry (Fig. 6d). Fault F16 is the major border fault and controls sag evolution. Faults F17 and F18 are synthetic faults and have little control over sediment filling. Although some antithetic faults (faults F19 and F20) develop in the slope area, they show small displacements and barely influence the sag architecture (Fig. 6d). The lowest depth of the Jurassic stratigraphy is *c.* 3100 m, whereas the thickness of pre-rift and syn-rift sediments is *c.* 2200 m (Fig. 6d). Bayanhua is the only sag with an east-dipping major border fault (fault F21) in the central sector (Figs 6e, 7). A synthetic fault (fault F22) (Fig. 6e) controls the sedimentary sequences in association with the major border fault (fault F21) and facilitates the horizontal propagation of the sag. Fault F21 declines in dip at a depth of *c.* 3300 m. Fault F22 bottoms out to F21 at a depth of *c.* 2400 m (Fig. 6e). Seismic data reveal that the lowest depth of the Jurassic stratigraphy is *c.* 2600 m and the thickness of pre-rift and syn-rift sediments is *c.* 1700 m (Fig. 6e). Sags in the central sector are generally narrow and characterized by shallow and short geometry.

The eastern sector is mainly composed of Holihe (10 in Fig. 7) and circumjacent small sags. Holihe is of length *c.* 75 km with a NE45° trending, and shows a width of *c.* 13 km (Fig. 6f, 7). It is composed of two sub-sags. A profile (Fig. 6f) crossing the south sub-sag indicates that the major border fault F23 and the subordinate antithetic fault F24 control the sedimentary filling in the faulted trough. Both of these faults show high-angle geometry at the shallow crust. The bottom depth of the Jurassic is *c.* 3400 m and the thickness of pre-rift and syn-rift sediments is *c.* 2800 m. Sags in this sector are of similar character to sags in the western sector (i.e. Chaokewula and Jiergalang): generally narrow and characterized by deep and long geometry.

https://doi.org/10.1017/S0016756817000267 Published online by Cambridge University Press

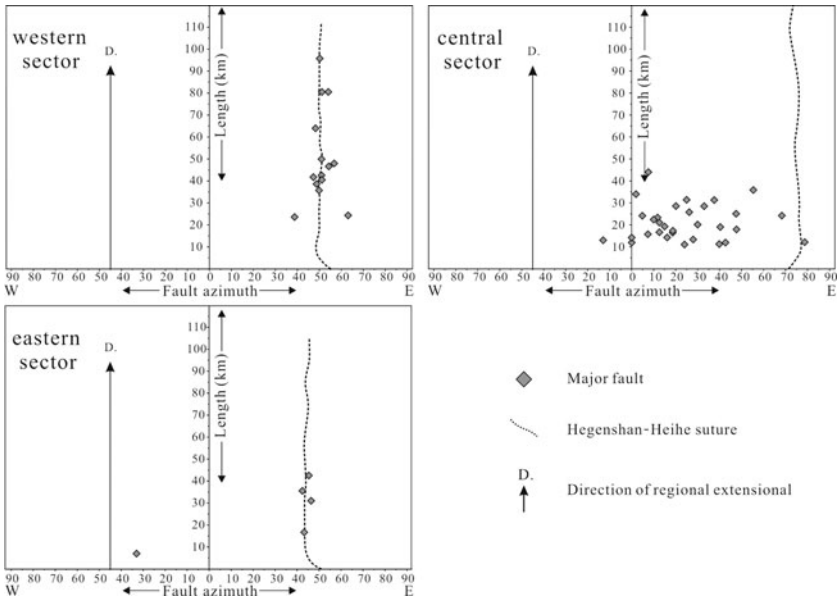

Figure 8. Length v. azimuth plots for the major faults and EHHS in western, central and eastern sectors of the Wunite Depression. D represents the regional extension in NW–SE direction. The plots show that most major faults follow the Hegenshan–Heihe suture in the western and eastern sectors, whereas most major faults are relatively scattered and at a high oblique angle to the Hegenshan–Heihe suture.

5. Relation between Hegenshan–Heihe suture and late Mesozoic extensional structures

Morley (1999) divided natural pre-existing structures into two main types: pervasive and discrete fabrics. Pervasive fabric commonly presents strong anisotropy throughout a large volume of rock; it is mostly preserved in metamorphic rocks as slaty cleavage or gneissic foliation. In the East African rift system, foliation preserved in the Precambrian basement (McConnell, 1972) is represented by a typically pervasive fabric. Discrete fabrics are the isolated planes or zones that display obviously different material behaviours than the surrounding rock. As the suture zone of the XMOB (Fig. 1b), they shows a different material behaviour than the Xing'an and Songliao blocks (Xu *et al.* 2015). It is therefore proposed that the Hegenshan–Heihe suture is a discrete pre-existing structure.

In the Wunite depression, the Hegenshan–Heihe suture is the main pre-existing structure, and the major faults (Fig. 7) are the main late Mesozoic extensional structure elements. We measured the horizontal length and orientation of the Hegenshan–Heihe suture. We also measured the horizontal length and orientation (fault-strike azimuth) of the major fault in the western, central and eastern sectors of the Wunite depression using seismic reflection data. The results were plotted as length v. azimuth graphs (Fig. 8). For the straight or slightly curved faults, we adopted the 'tip to tip' method used by Chattopadhyay & Chakra (2013). The method uses a straight line to join the two tips of the fault track. For a fault composed of several segments in an en échelon pattern, we measured the horizontal length and orientation of each segment separately. For the Hegenshan–Heihe suture, the horizontal azimuth was analysed based on the previous works, occurrence of ophiolites (Fig. 2) and geomagnetic anomaly (Fig. 3), we plotted this using a dotted line in each graph. The regional NW–SE direction of extension during the late Mesozoic is drawn using a solid line with an arrow.

In the western sector, the orientation of the Hegenshan–Heihe suture is *c.* NE50° and the angle between the suture and the regional direction of extension is *c.* 85°. The maximum frequency azimuth of major faults is *c.* NE50°, corresponding to the azimuth of the longest fault and the extension trend of the suture. The major faults occur at lower angles oblique to the direction of extension. The average length of major faults in the western sector is *c.* 45 km (Fig. 8a). In the central sector, the orientation of the Hegenshan–Heihe suture is *c.* NE75° and the angle between the suture and the regional direction of extension is *c.* 60°. The preponderant azimuth of major faults is NE0°–NE40° (Fig. 7). Most major faults are at 35–75° oblique to the suture, at 45°–85° oblique to the regional direction of extension. Typically, the lengths of major faults in the central sector are short; the average length of major faults is *c.* 22 km (Fig. 8b). In the eastern sector, the orientation of the Hegenshan–Heihe suture is *c.* NE45° and the angle between the suture and the regional direction of extension is *c.* 90°. The maximum frequency azimuth of major faults is *c.* NE45°, following the suture perpendicular to the regional direction of extension. The length of the longest fault in this sector is *c.* 36 km and the average length of the major faults is *c.* 30 km (Fig. 8c). Consequently, the data presented in Figure 8 indicate that major faults commonly follow the Hegenshan–Heihe suture and are longer in the western and eastern sectors; in the central sector they occur at high angles oblique to the Hegenshan–Heihe suture and are shorter.

https://doi.org/10.1017/S0016756817000267 Published online by Cambridge University Press

6. Discussion

6.a. Fault patterns compared to the analogue models

In the analogue models, the degree of oblique extension α is the angle between the direction of extension and the oblique trend at the basement of the model. For pure extension α = 90°, and for strike-slip α = 0° (Withjack & Jamison, 1986). The fault pattern in the eastern sector of the Wunite depression is reminiscent of the sandbox models of pure extension with α = 90° (Withjack & Jamison, 1986; McClay & White, 1995; Clifton *et al.* 2000). This suggests that the orthogonal rifting system develops in the eastern sector. The rift border fault is commonly formed by the linkage of small segments (Fig. 7). Both the rift border fault and subordinate antithetic fault formed parallel to the Hegenshan–Heihe suture and perpendicular to the direction of extension. The fault pattern in the western sector is similar to that in the eastern sector (Fig. 7). The rift border faults are composed of small segments. Both the border faults and intra-subordinate antithetic faults formed sub-parallel to the Hegenshan–Heihe suture and sub-perpendicular to the direction of extension. Although there is a slightly oblique angle (*c.* 5°) between the direction of extension and the Hegenshan–Heihe suture (Fig. 8a), we propose that an orthogonal rifting system also developed in the western sector.

In contrast, rift border faults in the central sector are highly segmented and form en échelon arrays parallel to the Hegenshan–Heihe suture. The angle between the direction of extension and the suture is *c.* 60° (Figs 7, 8b). According to the relation between the basement trend and the displacement direction, an overlying oblique rift system will develop. The fault pattern in the central sector will compare well with the analogue model of a moderately oblique extension with α = 60° (Withjack & Jamison, 1986; McClay & White, 1995; Clifton *et al.* 2000). However, in the central sector, the fault en échelon arrays are reminiscent of the moderately oblique extension with α = 60°, whereas the predominant strike of major faults is highly oblique to the suture (Fig. 8b). Compared with the moderately oblique extension experiment (Withjack & Jamison, 1986; McClay & White, 1995; Clifton *et al.* 2000), the predominant strike of faults is reoriented anticlockwise; the reorientation of the fault strike may have been influenced by the deformation of the Hegenshan–Heihe suture. During Early Cretaceous time, the Hegenshan–Heihe suture reactivated. The sinistral strike-slip deformation of the suture in the central sector may have resulted in the anticlockwise reorientation of the faults. The rotation process is detailed in the evolution model (Fig. 9).

6.b. Strain accommodation in the Wunite depression

Analogue experiments indicate that in orthogonal and low oblique rift systems the major rift border faults usually accrue most of the dip-slip deformation. In high oblique rift systems, the strain is usually partitioned and the major border faults accrue most of the strike-slip deformation (Withjack & Jamison, 1986; Bonini *et al.* 1997; Keep & McClay, 1997).

In the Wunite depression, the sags of the western and eastern sectors present orthogonal or suborthogonal rift features. The major border faults accrued most of the dip-slip motion. For example, from the seismic data fault F1 is the major border fault of Chaokewula sag. It accrues a vertical offset of at least *c.* 3300 m (Fig. 6a). Fault F6 in Jiergalang sag accrues a vertical offset of *c.* 4000 m (Fig. 6b) and Fault F23 in Holihe sag accrues a vertical offset of *c.* 3000 m (Fig. 6f). We cite laboratory experiments (Bonini *et al.* 1997; Keep & McClay, 1997) demonstrating that the major border faults accommodate most of the dip-slip motion. In addition, the effects of the subordinate antithetic faults resulted in the further vertical propagation of the sags.

In the central sector, the fault pattern presents an oblique rift feature. For example, in the Gaolihan sag, some subordinate faults are oblique to the major faults in plane (Gaolihan in Fig. 7). These subordinate faults form the en échelon fault zone with major faults 'Y'-shaped in seismic profile (Fig. 6c). The oblique rift feature reveals major faults in Gaolihan result in extensional deformation as well as strike-slip deformation. The strain is partitioned into strike-slip and dip-slip deformations. The decomposition of the strain resulted in the less-vertical offset of major faults.

Based on the thickness variation of strata from the seismic reflection data, the Gaolihan sag evolved after the early graben structures. During the pre-rift stage during Late Jurassic time, these structures exhibited a gentle variation in lateral thickness. Major border faults including F8, F9 and F10, and the antithetic fault F14, were the conjugate faults during the pre-rift stage that defined the early graben (Fig. 6c). During the syn-rift stage, Aershan and Tenggar formations, gradually thinning from east to west, were mainly deposited near faults F8, F9 and F10 and subordinate faults F12. The main reason may be that transtensional extension results in the localization of strain in the major border faults F8, F9 and F10 and subordinate faults F11, F12 and F13. The conjugated fault F14 was abandoned. The early graben evolved into a half-graben (Fig. 6c). An evolution process was proposed by Scholz & Contreras (1998): when the strain was localized, one of the major border faults was abandoned and the graben evolved into a half-graben. The same evolution characteristics can be distinguished in the Baoerguoji and Bayanhua sags (Fig. 6d, e).

6.c. Late Mesozoic evolution model of the Wunite depression

The distribution of late Mesozoic sags illustrates how the Wunite depression developed around the Hegenshan–Heihe suture. The analyses of the fault patterns and strain accommodation in this paper highlight the obvious differences in the late Mesozoic

https://doi.org/10.1017/S0016756817000267 Published online by Cambridge University Press

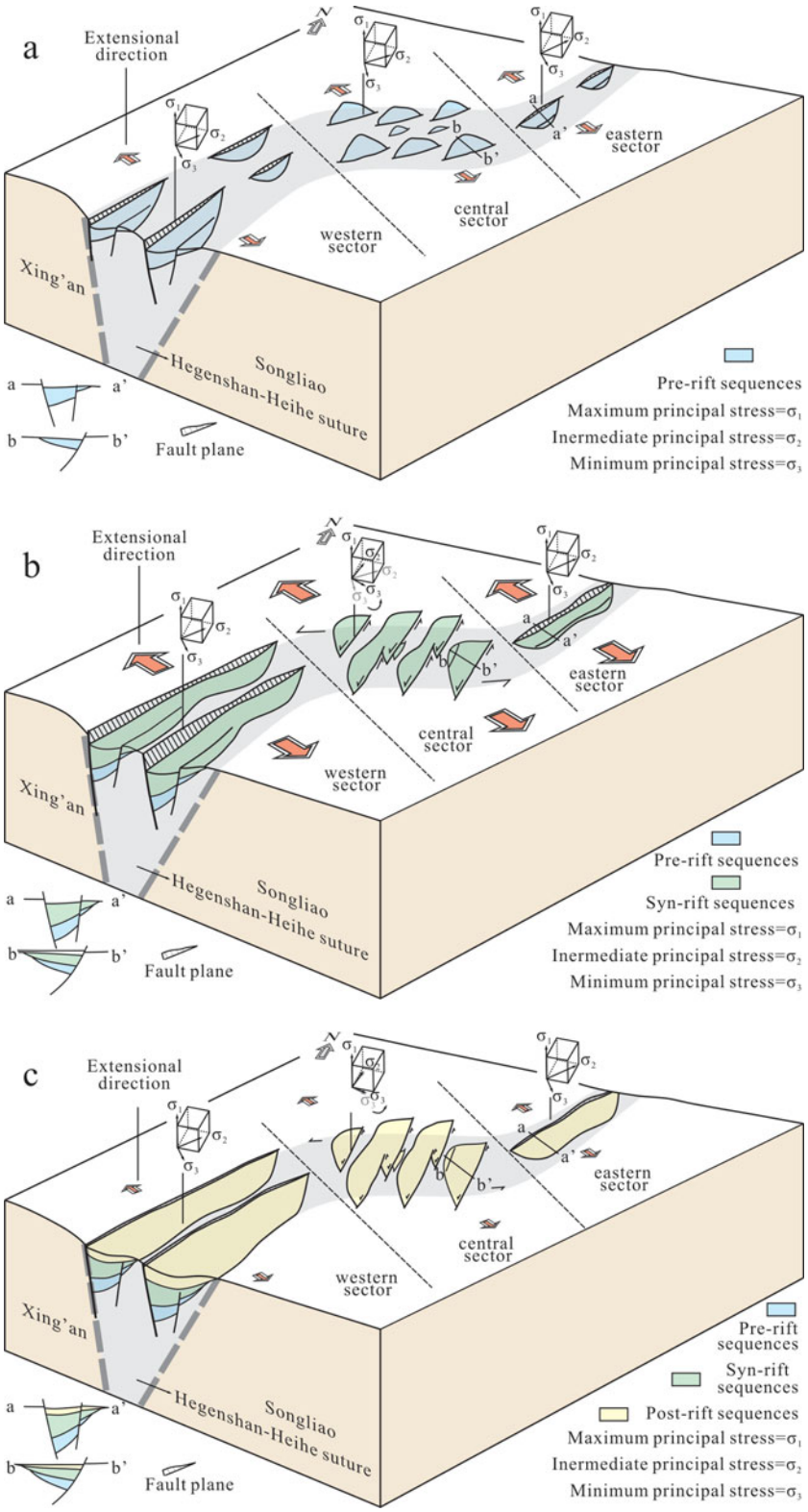

Figure 9. (Colour online) Evolution model showing the role of the Hegenshan–Heihe suture on the Late Mesozoic extensional structures, showing: (a) major faults in the western and eastern sectors mostly followed the suture, whereas major faults in the central sector were mostly at a low oblique angle to the suture during Late Jurassic time (pre-rift stage); (b) a strike rotation of the major faults in the central sector due to the sinistral strike-slip component of the reactivated suture during early Early Cretaceous time (syn-rift stage); and (c) the deformation of the suture decreased during late Early Cretaceous time (post-rift stage). Sags in the western and eastern sectors are deep and long, while sags in the central sector are shallow but short.

https://doi.org/10.1017/S0016756817000267 Published online by Cambridge University Press

extensional structures. Combining the geometry and kinematics of the pre-existing suture and the fault patterns and strain analyses, the role of the Hegenshan–Heihe suture in late Mesozoic extensional structures in the Wunite depression can be described by the evolution model in Figure 9. The Hegenshan–Heihe suture is the pre-existing suture that separates the Xing'an and Songliao blocks.

During Late Jurassic time (pre-rift stage) (Fig. 9a), a series of small fault segments followed the basement suture under the extension in a NW–SE direction. The orientations of minimum horizontal principal stress in the western and eastern sectors were sub-parallel–parallel to the regional direction of extension. The small segments were therefore sub-perpendicular–perpendicular to the regional direction of extension. In the central sector however, the orientation of minimum horizontal principal stress was oblique to the regional direction of extension. The small segments were in an en échelon array and oblique to the regional direction of extension (Fig. 9a). Variations in the orientations of minimum horizontal principal stress imply that, even if the regional extension direction is NW–SE, the principal stresses may differ locally. The local deflection of stress directions was due to the effects of the basement pre-existing structure. For instance, the Tertiary long fault trend in the Gulf of Thailand is N–S, whereas the short fault trend is NNE–SSW to NE–SE. Variations in the fault geometries are influenced by the pre-Tertiary structure (Morley *et al.* 2004). Due to the effects of the Hegenshan–Heihe suture sags in the western and eastern sectors presented orthogonal rift features, whereas in the central sector they presented oblique rift features.

During the increase of the regional extension during early Early Cretaceous time (syn-rift stage) (Fig. 9b), long faults were commonly formed by the linkage of small segments in the western and eastern sectors. The orientation of minimum horizontal principal stress was similar to that during Late Jurassic time (pre-rift stage). However, influenced by the Hegenshan–Heihe suture, the small fault segments in the central sector were prevented from linking with the long faults. Moreover, the dominant strike of the faults was re-oriented from NEE–SWW (following the Hegenshan–Heihe suture) to NNE–SSW. The azimuth of minimum horizontal principal stress changed from NNW–SSE to NWW–SEE (Fig. 9b). The sinistral nature of the horizontal principal stress was influenced by the deformation of the Hegenshan–Heihe suture, which was re-activated during early Early Cretaceous time. It mainly underwent extensional deformation in the western and eastern sectors under regional extension. Most extensional deformation accrued in the major border faults. The extensional deformation of the Hegenshan–Heihe suture therefore resulted in the further horizontal and vertical prolongation of faults. In the central sector, the transtensional extension of the Hegenshan–Heihe suture resulted in sinistral strike-slip deformation. The most sinistral strike-slip deformation accrued in the major border faults, whereas most dip-slip deformation accumulated in the subordinate faults. The sinistral strike-slip component induced the strike rotation of the minimum horizontal principal stress. Due to the strike-slip component, the extensional deformation of the major border faults was weak in the central sector. Moreover, the vertical displacements of major border faults were usually smaller than major border faults in the western and eastern sectors.

During late Early Cretaceous time (post-rift stage) (Fig. 9c), the deformation of the Hegenshan–Heihe suture significantly reduced with the decrease in regional extension. The displacements of the overlying major border faults were reduced further. In this stage, the orientations of the horizontal principal stress in the western, central and eastern sectors were basically the same as the early Early Cretaceous orientations (syn-rift stage). The architecture of the sags in the Wunite depression shows deep and long geometry in the western and eastern sectors, but shallow and short geometry in the central sector.

The architecture of the rift system may relate to the presence of the suture and rheology of the extending lithosphere (Corti *et al.* 2011). Series of the Baikal rift analogue models suggest that the presence of a near-vertical weak suture represents the more convenient rheological configuration, leading to a narrow rift depression. An increase in the difference in rheology beside the suture resulted in a striking increase in the asymmetry of the rift (Corti *et al.* 2011). By analogy with Baikal rift models (Corti *et al.* 2011), we propose that the Hegenshan–Heihe suture is a near-vertical pre-existing weak suture. It is the suture that results in the narrow rift system in the Wunite depression (Fig. 9). The asymmetrical degree of the rift may be basically influenced by the rheology of the two blocks beside the Hegenshan–Heihe suture. Along the axis of the Wunite depression, the asymmetrical degree of the sags in the central sector is higher than that of the sags in the western and eastern sectors. This may imply an increasing difference in rheology between the two blocks in the central sector.

Overall, the Hegenshan–Heihe suture influences the fault patterns and architecture of late Mesozoic sags in the Wunite depression. As the lithospheric weakness zone, it plays an important role in the later structures. The other Early Palaeozoic sutures in the XMOB (Fig. 1) may also be considered to be lithospheric weaknesses. The variant orientation and deformation may control the later deformation.

7. Conclusions

Analysis of architecture and fault patterns of sags based on the seismic reflection data has highlighted the importance of a pre-existing Hegenshan–Heihe suture in the evolution of the late Mesozoic rift system in the Wunite depression. (1) The development of sags that present as *c.* NE50° trending in the western sector was facilitated by the presence of a *c.* NE50°-trending

https://doi.org/10.1017/S0016756817000267 Published online by Cambridge University Press

Hegenshan–Heihe suture. The sags that present as *c.* NE45° trending in the eastern sector were controlled by the presence of a *c.* NE45°-trending suture. (2) The deep and long rift system in western and eastern sectors was mainly caused by the further extensional deformation of the suture during Early Cretaceous time. (3) The development of sags that present as *c.* NE0°–NE30° trending in the central sector were controlled by the *c.* NE75°-trending suture. (4) The transtensional extension of the reactivated suture resulted in the sinistral strike-slip component during Early Cretaceous time. This facilitated the clockwise strike reorientation of major border faults. (5) The sinistral strike-slip deformation of the suture led to most sinistral strike-slip motion accruing in the major border faults. The less-vertical offset therefore resulted in the shallow rift system.

Acknowledgements. This work is funded by the National Science and Technology Major Project No. 2011ZX05009–001. Grateful acknowledgements are made to the exploration department of PetroChina Huabei Oilfield Company, which contributed cores and seismic data for this work. We also gratefully acknowledge the constructive reviews from Professor Chiara Frassi. Our heartfelt gratitude also goes to reviewers for their scientific and linguistic revisions of the manuscript.

References

Badarch, G., Gunningham, W. D. & Windley, B. F. 2002. A new terrane subdivision for Mongolia: implications for the Phanerozoic crustal growth of Central Asia. *Journal of Asian Earth Science* **21**, 87–110.

Bonini, M., Souriot, T.Boccaletti, M. & Brun, J. P. 1997. Successive orthogonal and oblique extension episodes in a rift zone: laboratory experiments with application to the Ethiopian Rift. *Tectonics* **16**, 347–62.

Chattopadhyay, A. & Chakra, M. 2013. Influence of pre-existing pervasive fabrics on fault patterns during orthogonal and oblique rifting: an experimental approach. *Marine and Petroleum Geology* **39**, 74–91.

Chen, Y. & Chen, W. 1997. *Mesozoic Volcanic Rocks: Chronology, Geochemistry and Tectonic Background*. Beijing: Seismology Press, 279 pp. (in Chinese with English abstract).

Clifton, A. E., Schlische, R. W., Withjack, M. O. & Ackermann, R. V. 2000. Influence on rift obliquity on fault-population systematics: results of experimental clay models. *Journal of Structural Geology* **22**, 1491–509.

Corti, G., Calignano, E., Petit, C. & Sani, F. 2011. Controls of lithospheric structure and plate kinematics on rift architecture and evolution: an experimental modeling of the Baikal rift. *Tectonics* **30**, 70–82.

Dewey, J. F. 1977. Suture zone complexities: a review. *Tectonophysics* **40**, 53–7.

Dooley, T., McClay, K. R. & Pascoe, R. 2003. 3D analogue models of variable displacement extensional faults, applications to the Revfallet fault system, offshore mid-Norway. In: *New Insights into Structural Interpretation and Modelling* (ed. D. A. Nieuwland), pp. 151–67. Geological Society, London, Special Publication no. 212.

Dou, L. R. 1997. The Lower Cretaceous Petroleum System in NE China. *Journal of Petroleum Geology* **20**, 475–88.

Dou, L. R. & Chang, L. A. 2003. Fault linkage patterns and their control on the formation of the petroleum systems of the Erlian Basin, Eastern China. *Marine and Petroleum Geology* **20**, 1213–24.

Dunbar, J. A. & Sawyer, D. S. 1988. Continental rifting at pre-existing lithosphere weaknesses. *Nature* **333**, 450–52.

Fei, B. S. 1985. Tectonic evolution of the Erlian Basin and its bearing on oil and gas. *Geotectonic et Metallogenia* **9**, 121–31 (in Chinese with English abstract).

Feng, Z. Q., Liu, Y. J., Han, G. Q., Wen, Q. B., Li, W. M. & Zhang, L. 2014. The petrogenesis of ∼330 Ma metagabbro-granite from the Tayuan area in the northern segment of the Da Xing'an Mts and its tectonic implication. *Acta Petrologica Sinica* **30**, 1982–94 (in Chinese with English abstract).

Feng, Z. Q., Liu, Y. I., Liu, B. Q., Wen, Q. B., Li, W. M. & Liu, Q. 2016. Timing and nature of the Xinlin-Xiguitu Ocean: constraints from ophiolitic gabbros in the northern Great Xing'an Range, eastern Central Asian Orogenic Belt. *International Journal of Earth Sciences* **105**(2), 491–505.

Ge, W. C., Wu, F. Y., Zhou, C. Y. & Abdel Rahman, A. A. 2005. Emplacement age of the Tahe granite and its constraints on the tectonic nature of the Erguna block in the northern part of the Da Xing'an Rang. *Chinese Science Bulletin* **50**, 2097–105 (in Chinese with English abstract).

Graham, S. A., Hendrix, M. S., Johnson, C. L., Badamgarav, D., Badarch, G., Amory, J., Porter, M., Barsbold, R., Webb, L. E. & Hacker, B. R. 2001. Sedimentary record and tectonic implications of Mesozoic rifting in southeast Mongolia. *Geological Society of America Bulletin* **113**, 1560–79.

Han, G., Liu, Y., Neubauer, F., Bartel, E., Genser, J., Feng, Z., Zhang, L. & Yang, M. 2015. U–Pb age and Hf isotopic data of detrital zircons from the Devonian and Carboniferous sandstones in Yimin area, NE China: new evidences to the collision timing between the Xing'an and Erguna blocks in eastern segment of Central Asian Orogenic Belt. *Journal of Asian Earth Sciences* **97**, 211–28.

Han, G., Liu, Y. J., Neubauer, F., Jin, W., Genser, J., Ren, S. M., Li, W., Wen, Q. B., Zhao, Y. L. & Liang, C. Y. 2012. LA-ICP-MS U–Pb dating and Hf isotopic compositions of detrital zircons from the Permian sandstones in Da Xing'an Mountains, NE China: new evidence for the eastern extension of the Erenhot–Hegenshan suture zone. *Journal of Asian Earth Sciences* **49**, 249–71.

Han, J., Zhou, J. B., Wang, B. & Cao, J. L. 2015. The final collision of the CAOB: constraint from the zircon U–Pb dating of the Linxi Formation, Inner Mongolia. *Geoscience Frontiers* **6**, 211–25.

Higgins, R. L. & Harris, L. B. 1997. The effect of cover composition on extensional faulting above reactivated basement faults: results from analogue modeling. *Journal of Structural Geology* **19**, 89–98.

Jian, P., Kröner, F., Windley, B. F., Shi, Y. R., Zhang, W., Zhang, L. Q. & Yang, W. R. 2012. Carboniferous and Cretaceous mafic-ultra mafic massifs in Inner Mongolia (China): a SHRIMP zircon and geochemical study of the previously presumed integral "Hegenshan ophiolite". *Lithos* **142**–3, 48–66.

Jian, P., Liu, D. Y., Kröner, A., Windley, B. F., Shi, Y. R., Zhang, W., Zhang, F. Q., Miao, L. C., Zhang, L. Q.

& Tomurhuu, D. 2010. Evolution of a Permian intraoceanic arc-trench system in the Solonker suture zone, Central Asian Orogenic Belt, China and Mongolia. *Lithos* **118**, 169–90.

Jutz, S. L. & Chorowicz, J. 2010. Geological mapping and detection of oblique extensional structures in the Kenyan Rift Valley with a SPOT/Landsat-TM datamerge. *Australian Journal of Earth Science* **14**, 1677–88.

Keep, M. & McClay, K. R. 1997. Analogue modeling of multiphase rift systems. *Tectonophysics* **273**, 239–70.

Kuang, H. W., Liu, Y. Q., Liu, Y. X., Peng, N., Xu, H., Dong, C., Liu, H., Xu, J. L. & Xue, P. L. 2013. Stratigraphy and depositional palaeogeography of the Early Cretaceous basins in Da Hinggan Mountains–Mongolia orogenic belt and its neighboring areas. *Geological Bulletin of China* **32**, 1063–84 (in Chinese with English abstract).

Lasky, R. P. & Glikson, A. Y. 2011. Gnargoo: a possible 75 km-diameter post-Early Permian – pre-Cretaceous buried impact structure, Carnarvon Basin, Western Australia. *Australian Journal of Earth Science* **48**, 131–49.

Li, C., Xiao, W. J., Han, C. M., Zhou, K. F., Zhang, J. E. & Zhang, Z. X. 2014. Late Devonian–early Permian accretionary orogenesis along the North Tianshan in the southern Central Asian Orogenic Belt. *Australian Journal of Earth Science* **57**, 1023–50.

Li, J. Y. 1998. Some new ideas on tectonics of NE China and its neighboring areas. *Geological Review* **44**, 339–47 (in Chinese with English abstract).

Li, J. Y. 2006. Permian geodynamic setting of Northeast China and adjacent regions: closure of the Paleo-Asian Ocean and subduction of the Paleo-Pacific Plate. *Journal of Asian Earth Sciences* **26**, 207–24.

Li, J. Y., Zhang, J., Yang, T. N., Li, Y. P., Sun, G. H., Zhu, Z. X. & Wang, L. J. 2009. Crustal tectonic division and evolution of the southern part of the North Asian Orogenic Region and its adjacent areas. *Journal of Jilin University (Earth Science Edition)* **39**, 584–05 (in Chinese with English abstract).

Li, S. T., Lu, F. X. & Lin, C. S. 1997. *Evolution of Mesozoic and Cenozoic Basins in Eastern China and their Geodynamic Background*. Wuhan: China University of Geosciences Press, 239 pp. (in Chinese with English abstract).

Lin, C. S., Eriksson, K., Li, S. T., Wang, Y. X., Ren, J. Y. & Zhang, Y. M. 2001. Sequence architecture, depositional systems, and controls on development of lacustrine basin fills in part of the Erlian Basin, northeast China. *AAPG Bulletin* **85**, 2017–43.

Liu, Y. J., Li, W. M., Feng, Z. Q., Wen, Q. B., Neubauer, F. & Liang, C. Y. 2017. A review of the Paleozoic tectonics in the eastern part of Central Asian Orogenic Belt. *Gondwana Research* **43**, 123–48.

Luo, Z.L., Li, J.M. & Liu, S.G. 2005. *Plate Tectonics and Analysis of Petroliferous Basins in China*. Beijing: Petroleum Industry Press, 643 pp. (in Chinese with English abstract).

Ma, X. Y., Liu, H. F., Wang, W. X. & Wang, Y. P. 1983. Meso-Cenozoic taphrogeny and extensional tectonics in eastern China. *Acta Geologica Sinica* **56**, 22–32.

McClay, K. R. & White, M. J. 1995. Analogue modeling of orthogonal and oblique rifting. *Marine and Petroleum Geology* **12**, 137–51.

McConnell, R. B. 1972. Geological development of the rift system of eastern Africa. *Geological Society of America Bulletin* **83**, 2549–72.

Meng, Q. A., Zhu, D. F., Chen, J. L. & Qi, J. F. 2012. Styles of complex faulted sags in rifting basin and its significance for petroleum geology: an example from Hailar–Tamsag Early Cretaceous Basin. *Earth Science Frontiers* **19**, 76–85 (in Chinese with English abstract).

Meng, Q. R. 2003. What drove late Mesozoic extension of the northern China–Mongolia tract? *Tectonophysics* **369**, 155–74.

Meng, Q. R., Hu, J. M., Jin, J. Q., Zhang, Y. & Xu, D. F. 2003. Tectonics of the late Mesozoic wide extensional basin system in the China–Mongolia border region. *Basin Research* **15**, 397–415.

Meng, Q. R., Hu, J. M., Yuan, X. J. & Qin, J. Q. 2002. Structure, evolution and origin of Late Mesozoic extensional basins in the China–Mongolia border region. *Geological Bulletin of China* **21**, 224–31 (in Chinese with English abstract).

Meng, Q. R., Wei, H. H., Wu, G. L. & Duan, L. 2013. Early Mesozoic tectonics settings of the northern North China Craton. *Tectonophysics* **611**, 155–66.

Miao, L. C., Fan, W. M., Liu, D. Y., Zhang, F. Q., Shi, Y. R. & Guo, F. 2008. Geochronology and geochemistry of the Hegenshan ophiolitic complex: implications for late-stage tectonic evolution of the Inner Mongolia–Daxinganling Orogenic belt, China. *Journal of Asian Earth Sciences* **32**, 348–70.

Miao, L. C., Fan, W. M., Zhang, F. Q., Liu, D. Y., Jian, P., Shi, G. H., Tao, H. & Shi, Y. R. 2004. Zircon SHRIMP geochronology of the Xinkailing-Kele complex in the northwestern Lesser Xing'an Range, and its geological implications. *Chinese Science Bulletin* **49**, 201–9.

Miao, L. C., Liu, D. Y., Zhang, F. Q., Fan, W. M., Shi, Y. R. & Xie, H. Q. 2007. Zircon SHRIMP U–Pb ages of the "Xinghuadukou Group" in Hanjiayuanzi and Xinlin areas and the "Zhalantun Group" in Inner Mongolia, Da Hinggan Mountains. *Chinese Science Bulletin* **52**, 1112–24.

Milani, E. J. & Davison, I. 1988. Basement control and transfer tectonics in the Recôncavo–Tucano–Jatobá rift, Northeast Brazil. *Tectonophysics* **154**, 41–50, 53–70.

Morley, C. K. 1999. How successful are analogue models in addressing the influence of pre-existing fabrics on rift structure? *Journal of Structural Geology* **21**, 1267–74.

Morley, C. K., Haranya, C., Phoosongsee, W., Pongwapee, S., Kornsawan, A. & Wonganan, N. 2004. Activation of rift oblique and rift parallel pre-existing fabrics during extension and their effect on deformation style: examples from the rifts of Thailand. *Journal of Structural Geology* **26**, 1803–29.

Nozaka, T. & Liu, Y. 2002. Petrology of the Hegenshan ophiolite and its implications for the tectonic evolution of northern China. *Earth and Planetary Science Letters* **202**, 89–104.

Qi, J. F., Zhao, X. Z., Li, X. P., Yang, M. H., Xiao, Y., Yu, F. S. & Dong, Y. Q. 2015. The distribution and relationship between Early Cretaceous sags and their relationship with basement structure within Erlian Basin. *Earth Science Frontiers* **22**, 118–28 (in Chinese with English abstract).

Quinlan, G., Walsh, J., Skogseid, J., Sassi, W., Cloetingh, S., Lobkovsky, L., Bois, C., Stel, H. & Banda, E. 1993. Relationship between deeper lithospheric processes and near-surface tectonics of sedimentary basins. *Tectonophysics* **226**, 217–25.

Ratschbacher, L., Hacker, B. R., Webb, L. E., Mcwilliams, M., Ireland, T., Dong, S., Calvert, A., Chateigner, D. & Wenk, H. R. 2000. Exhumation of the ultrahigh-pressure continental crust in east central

China: Cretaceous and Cenozoic unroofing and the Tan–Lu fault. *Journal of Geophysical Research, Solid Earth* **105**, 13303–38.

Ren, J. Y., Li, S. T. & Jiao, G. H. 1998. Extensional tectonic system of Erlian Fault Basin Group and its deep background. *Earth Science–Journal of China University of Geosciences* **23**, 567–72 (in Chinese with English abstract).

Robinson, P. T., Bai, W. J., Yang, J. S., Hu, X. F. & Zhou, M. F. 1995. Geochemical constraints on the petrogenesis and crustal accretion of the Hegenshan Ophiolite, northern China. *Acta Petrologica Sinica* **11**, 112–24 (in Chinese with English abstract).

Robinson, P. T., Zhou, M. F., Hu, X. F., Reynolds, P. & Bai, W. J. 1999. Geochemical constraints on the origin of the Hegenshan ophiolite, Inner Mongolia, China. *Journal of Asian Earth Sciences* **17**, 423–42.

Rosenberg, C. L., Brun, J. P., Cagnard, F. & Gapais, D. 2007. Oblique indentation in the Eastern Alps: insights from laboratory experiments. *Tectonics* **26**, 1–23.

Schlische, R. W., Withjack, M. O. & Eisenstakt, G. 2002. An experimental study of the secondary deformation produced by oblique-slip normal faulting. *AAPG Bulletin* **86**, 885–906.

Scholz, C. H. & Contreras, J. C. 1998. Mechanics of continental rift architecture. *Geology* **26**, 967–70.

Şengör, A. M. C. 1992. The Paleo-Tethyan suture: a line of demarcation between two fundamentally different architectural styles in the structure of Asia. *Island Arc* **1**, 78–91.

Sengör, A. M. C., Natal'in, B. A. & Burtman, V. S. 1993. Evolution of the Altaid tectonic collage and Paleozoic crustal growth in Eurasia. *Nature* **364**, 299–307.

Shao, J. A., Mu, B. L. & Zhang, L. Q. 2000. Deep geological process and its shallow response during Mesozoic transfer of tectonic frameworks in eastern North China. *Geological Review* **46**, 32–40 (in Chinese with English abstract).

Shi, Y. R., Anderson, J. L., Li, L. L., Ding, J., Zhang, W. & Shen, C. H. 2016. Zircon ages and Hf isotopic compositions of Permian and Triassic A-type granites from central Inner Mongolia and their significance for late Paleozoic and early Mesozoic evolution of the Central Asian Orogenic Belt. *Australian Journal of Earth Science* **58**, 967–82.

Song, J. & Dou, L. 1997. *Mesozoic–Cenozoic Tectonics of Petroliferous Basins in Eastern China and their Petroleum Systems*. Beijing: Petroleum Industry Press, 182 pp. (in Chinese with English abstract).

Su, B. X., Qin, K. Z., Sakyi, P. A., Malaviarachchi, S. P. K., Liu, P. P., Tang, D. M., Xiao, Q. H., Sun, H., Ma, Y. G. & Mao, Q. 2012. Occurrence of an Alaskan-type complex in the Middle Tianshan Massif, Central Asian Orogenic Belt: inferences from petrological and mineralogical studies. *Australian Journal of Earth Science* **54**, 249–69.

Sun, D. Y., Wu, F. Y., Zhang, Y. B. & Gao, S. 2004. The final closing time of the west Lamulun River-Changchun-Yanji plate suture zone: evidence from the Dayushan granitic pluton, Jilin Province. *Journal of Jilin University (Earth Science Edition)* **34**, 174–81 (in Chinese with English abstract).

Sun, W., Chi, X. G., Zhao, Z., Pan, S. Y., Liu, J. F., Zhang, R. & Quan, J. Y. 2014. Zircon geochronology constraints on the age and nature of 'Precambrian metamorphic rocks' in the Xing'an block of Northeast China. *International Geology Review* **56**(6), 672–94.

Sun, Y. W., Li, M. S., Ge, W. C., Zhang, Y. L. & Zhang, D. J. 2013. Eastward termination of the Solonker–Xar Moron River Suture determined by detrital zircon U–Pb isotopic dating and Permian floristics. *Journal of Asian Earth Sciences* **75**, 243–50.

Tong, H. M. & Yin, A. 2011. Reactivation tendency analysis: a theory for predicting the temporal evolution of pre-existing weakness under uniform stress state. *Tectonophysics* **503**, 195–200.

Tong, H. M., Koyi, H., Huang, S. & Zhao, H. T. 2014. The effect of multiple pre-existing weaknesses on formation and evolution of faults in extended sandbox models. *Tectonophysics* **626**, 197–212.

Tortorici, L., Catalano, S. & Carmelo, M. 2008. Phiolite-bearing mélanges in southern Italy. *Geological Journal* **44**, 153–66.

Traynor, J. J. & Sladen, C. 1995. Tectonic and stratigraphic evolution of the Mongolian People's Republic and its influence on hydrocarbon geology and potential. *Marine and Petroleum Geology* **12**, 35–2.

Wang, F., Zhou, X. H., Zhang, L. C., Ying, J. F., Zhang, Y. T., Wu, F. Y. & Zhu, R. X. 2006. Late Mesozoic volcanism in the Great Xing'an Range (NE China): Timing and implications for the dynamic setting of NE Asia. *Earth and Planetary Science Letters* **251**, 179–198.

Wang, T. 1986. A preliminary study on the Erlian Basin characteristics for structural petroleum geological. *Experimental Petroleum Geology* **8**, 313–324 (in Chinese with English abstract).

Wang, T., Zheng, Y. D., Zhang, J. J., Wang, X. S., Zeng, L. S. & Tong, Y. 2007. Some problems in the study of Mesozoic extensional structure in the North China Craton and its significance for the study of lithospheric thinning. *Geological Bulletin of China* **26**, 1154–1166 (in Chinese with English abstract).

Wang, Y. D., Sun, F. Y., Li, L., Li, R. H., Wang, J. & Xin, W. 2015. Geochronology, geochemistry, and geological implications of late Carboniferous–early Permian mafic and felsic intrusive rocks from Urad Zhongqi, western Inner Mongolia. *Geological Magazine* **152**, 1057–72.

Wang, Y. J. & Fan, Z. Y. 1997. Discovery of Permian radiolarians in Ophiolite Belt on northern side of Xar Moron River, Nei Monggol and its geological significance. *Acta Palaeontologica Sinica* **36**, 58–69 (in Chinese with English abstract).

Watson, M. P., Hayward, A. B., Parkinson, D. N. & Zhang, Z. M. 1987. Plate tectonic history, basin development and petroleum source rock deposition onshore China. *Marine and Petroleum Geology* **4**, 205–25.

Webb, L. E., Graham, S. A., Johnson, C. L., Badarch, G. & Hendrix, M. S. 1999. Occurrence, age, and implications of the Yagan–Onch Hayrhan metamorphic ocre complex southern Mongolia, *Geology* **27**, 143–46.

Wilhem, C., Windley, B. F. & Stampfli, G. M. 2012. The Altaids of Central Asia: a tectonic and evolutionary innovative review. *Earth-Science Reviews* **113**, 303–41.

Windley, B. F., Alexeiev, D., Xiao, W. J., Kröner, A. & Bombosuren, B. 2007. Tectonic models for accretion of the Central Asian Orogenic Belt. *Journal of the Geological Society* **164**, 31–47.

Withjack, M. O. & Jamison, W. R. 1986. Deformation produced by oblique rifting. *Tectonophysics* **126**, 99–124.

Wu, F. Y., Sun, D. Y. & Lin, Q. 1999. Petrogenesis of the Phanerozoic granites and crustal growth in the northeast China. *Acta Petrologica Sinica* **15**, 181–9.

https://doi.org/10.1017/S0016756817000267 Published online by Cambridge University Press

Wu, F. Y., Yang, J. H., Lo, C. H., Wilde, S. A., San, D. Y. & Jahn, B. M. 2007. The Heilongjiang Group: a Jurassic accretionary complex in the Jiamusi Massif at the western Pacific margin of northeastern China. *Island Arc* **16**, 156–72.

Xiao, A. C., Yang, S. F. & Chen, H. L. 2001. Geodynamic background on formation of Erlian Basin. *Oil & Gas Geology* **22**, 137–40 (in Chinese with English abstract).

Xiao, W., Sun, M. & Santosh, M. 2015. Continental reconstruction and metallogeny of the Circum-Junggar areas and termination of the southern Central Asian Orogenic Belt. *Geoscience Frontiers* **6**, 137–40.

Xiao, W. J., Han, C. M., Liu, W., Wan, B., Zhang, J. E., Ao, S. J., Zhang, Z. Y., Song, D. F., Tian, Z. H. & Luo, J. 2014. How many sutures in the southern Central Asian Orogenic Belt: insights from East Xinjiang–West Gansu (NW China)? *Geoscience Frontiers* **5**, 525–36.

Xiao, W. J., Kröner, A. & Windley, B. 2009. Geodynamic evolution of Central Asia in the Paleozoic and Mesozoic. *International Journal of Earth Sciences* **98**, 1185–8.

Xiao, W. J., Windley, B. F., Hao, J. & Zhai, M. G. 2003. Accretion leading to collision and the Permain Solonker suture, Inner Mongolia, China: termination of the central Asian orogenic belt. *Tectonics* **22**, 288–308.

Xu, B., Zhao, P., Wang, Y. Y., Liao, W., Luo, Z.W., Bao, Q. Z. & Zhou, Y. H. 2015. The pre-Devonian tectonic framework of Xing'an–Mongolia orogenic belt (XMOB) in north China. *Journal of Asian Earth Sciences* **97**, 183–96.

Yu, Y. T. 1990. Evolution characteristics of Erlian Basin and the distribution of oil and gas deposits. *Acta Petrolei Sinica* **11**, 12–20 (in Chinese with English abstract).

Zeng, Q. D., Liu, J. M., Chu, S. X., Wang, Y. B., Sun, Y., Duan, X. X. & Zhou, L. L. 2012. Mesozoic molybdenum deposits in the East Xingmeng orogenic belt, northeast China: characteristics and tectonic setting. *Australian Journal of Earth Science* **54**, 1843–69.

Zhang, L., Liu, Y. J., Li, W. M., Han, G. Q., Zhang, J. D., Guo, Q. Y. & Li, C. H. 2013. Discussion of the basement properties and east boundary of the Erngun massif. *Chinese Journal of Geology* **48**, 227–44 (in Chinese with English abstract).

Zhang, S., Gao, R., Li, H., Hou, H. S., Wu, H. C., Li, W. S., Yang, K., Li, C., Li, W. H., Zhang, J. S., Yang, T. S., Keller, G. R. & Liu, M. 2014. Crustal structures revealed from a deep seismic reflection profile across the Solonker suture zone of the Central Asian Orogenic Belt, northern China: an integrated interpretation. *Tectonophysics* **612–3**, 26–39.

Zhang, W. C. 1998. Sedimentary facies and hydrocarbon-bearing of Lower Cretaceous strata in Erlian Basin. *Scientia Geologica Sinica* **33**, 204–13.

Zhang, X. Z., Yang, B. J., Wu, F. Y. & Liu, X. G. 2006. The lithosphere structure in the Hingmong-Jihei (Hinggan-Mongolia-Heilongjiang) region, northeastern China. *Geology in China* **33**, 816–23 (in Chinese with English abstract).

Zhang, Y. X., Sun, Y. S., Zhang, X. Z., Yang, B. J. & Jin, X. 1994. *The 1:1,000,000 Specification of the Manzhouli–Suifenhe Geotransect*. Beijing: Geological Publishing House, 53 pp. (in Chinese with English abstract).

Zheng, Y. D., Wang, S. Z. & Wang, Y. F. 1991. An enormous thrust nappe and extensional metamorphic core complex newly discovered in Sino–Mongolian boundary area. *Science in China Series B* **34**, 1145–52.

Zhou, J. B., Cao, J. L, Wilde, S. M., Zhao, G. C., Zhang, J. J. & Wang, B. 2014. Paleo-Pacific subduction-accretion: evidence from Geochemical and U-Pb zircon dating of the Nadanhada accretionary complex, NE China. *Tectonics* **33**, 2444–66.

Zhou, J. B., Han, J., Zhao, G. C., Zhang, X. Z., Cao, J. L., Wang, B. & Pei, S. H. 2015. The emplacement time of the Hegenshan ophiolite: constraints from the unconformably overlying Paleozoic strata. *Tectonophysics* **662**, 398–415.

Zhou, J. B., Wilde, S. A., Zhang, X. Z., Ren, S. M. & Zheng, C. Q. 2011. Early Paleozoic metamorphic rocks of the Erguna block in the Great Xing'an Rang, NE China: evidence for the timing of magmatic and metamorphic events and their tectonic implications. *Tectonophysics* **499**, 105–17.

Zhu, D., Wu, Z., Cui, S., Wu, G., Ma, Y. Y. & Feng, X. 1999. Features of Mesozoic magmatic activities in the Yanshan area and their relation to intracontinental orogenesis. *Geological Review* **45**, 165–72.